THE JOURNAL OF BIOLOGICAL CHEMISTRY VOL. 291, NO. 45, pp. 23604–23617, November 4, 2016

TCL/RhoJ Plasma Membrane Localization and Nucleotide Exchange Is Coordinately Regulated by Amino Acids within the N Terminus and a Distal Loop Region*

Received for publication, July 22, 2016, and in revised form, September 19, 2016 Published, JBC Papers in Press, September 22, 2016, DOI 10.1074/jbc.M116.750026

Karly L. Ackermann, Rebecca R. Florke, Shannon S. Reyes, Brooke R. Tader, and Michael J. Hamann[1]

From the Biology Department, Bemidji State University, Bemidji, Minnesota 56601

Edited by Henrik Dohlman

TCL/RhoJ is a Cdc42-related Rho GTPase with reported activities in endothelial cell biology and angiogenesis, metastatic melanoma, and corneal epithelial cells; however, less is known about how it is inherently regulated in comparison to its closest homologues TC10 and Cdc42. TCL has an N-terminal extension of 18 amino acids in comparison to Cdc42, but the function of this amino acid sequence has not been elucidated. A truncation mutant lacking the N terminus (ΔN) was found to alter TCL plasma membrane localization and nucleotide binding, and additional truncation and point mutants mapped the alterations of TCL biochemistry to amino acids 17–20. Interestingly, whereas the TCL ΔN mutant clearly influenced nucleotide exchange, deletion of the N terminus from its closest homologue, TC10, did not have a similar effect. Chimeras of TCL and TC10 revealed amino acids 121–129 of TCL contributed to the differences in nucleotide loading. Together, these results identify amino acids within the N terminus and a loop region distal to the nucleotide binding pocket of TCL capable of allosterically regulating nucleotide exchange and thus influence membrane association of the protein.

TCL/RhoJ was first characterized about 15 years ago as a Rho GTPase with closest sequence homology to TC10 and Cdc42 and so was termed TCL for being "TC10-like." Its primary sequence shares the G-domains found within the Rho family GTPases that facilitate binding of guanine nucleotides and hydrolysis of the γ-phosphate from guanosine triphosphate (1). Its similarity to Cdc42 indicated at the time of its initial characterization that it had some potential for redundant functionality, particularly because TCL interacts with some of the same downstream effector proteins such as PAK[2] and Wiskott-Aldrich Syndrome protein (1, 2). These initial observations pointed to TCL behaving as a typical Rho family GTPase, with GDP-loaded TCL functioning as the inactive form of the protein, whereas GTP-loaded TCL stimulates downstream signaling by interacting with appropriate actin remodeling effector proteins (3).

Early attempts to frame the cellular context of the function of TCL implicated it in vesicle transport and recycling pathways associated with clathrin-mediated endocytosis, with TCL facilitating the return of receptors to the plasma membrane after internalization (4). More recently, TCL expression was shown to be amplified in endothelial cells, potentially through the influence of the transcription factor ERG, where it participates in the projection and lumenization of new vessels (5–9). TCL also has a unique role in tumor-associated angiogenesis and in the maintenance of a stable tumor vasculature suggesting TCL may prove to be a reasonable chemotherapeutic target. This notion has been supported using directed delivery of siRNAs against TCL to endothelial cells of nude mice bearing human tumor explants. TCL suppression in these experiments inhibited pro-angiogenic vessel infiltration of tumors and promoted a loss of vessel integrity within the tumor mass (10). TCL expression and activity has also been implicated in metastatic melanomas, conferring both chemo-resistance and enhanced motility to the cancer cells (11, 12). These unique niches of TCL activity suggest it is a strong candidate for directed chemotherapy, with few anticipated off-target effects, particularly as TCL knock-out mice show little phenotypic impairments except minor defects in corneal development (10, 13).

Little is known about the molecular pathways that facilitate the function of TCL, and except for a few investigations, there is limited evidence regarding how nucleotide binding and hydrolysis may be influenced by GEFs and GAPs (8, 14, 15). In terms of relevant binding partners, TCL has been shown to directly interact with the GIT-PIX protein complex, leading to enhanced stabilization of focal adhesions. The interaction may be required to enhance endothelial tube formation during angiogenesis, as either GIT-PIX or TCL suppression resulted in reduced human umbilical vein endothelial cells tubule loop formations *in vitro*. However, it is unclear how the interaction is initiated and whether TCL is required for other pro-angiogenesis processes (16).

To better understand the inherent biochemical properties of TCL that lead to its cellular activation, we sought to perform a more thorough structure/function analysis of the GTPase, partly in the hope of uncovering unique, targetable sites for anti-angiogenesis therapies (10). Our strategy was to pursue

* The authors declare that they have no conflicts of interest with the contents of this article. The content is solely the responsibility of the authors and does not necessarily represent the official views of the National Institutes of Health.

[1] To whom correspondence should be addressed: Bemidji State University, 1500 Birchmont Dr. NE #27, Bemidji, MN 56601. Tel.: 218-755-2798; Fax: 218-755-4107; E-mail: mhamann@bemidjistate.edu.

[2] The abbreviations used are: PAK, p21-activated kinase; GAP, GTPase-activating protein; GEF, guanine nucleotide exchange factor; EEA1, early endosomal antigen 1; mant-GTP, 2′(3′)-*O*-(*N*′-methylanthraniloyl)-GTP; SH3, Src homology; aa, amino acid(s).

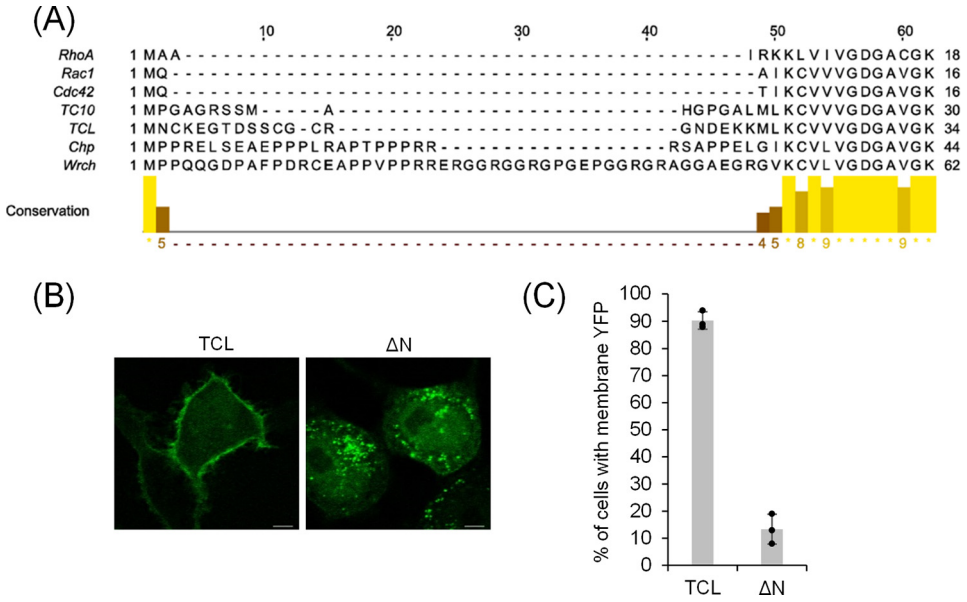

FIGURE 1. **The N terminus of TCL regulates its subcellular localization.** *A,* a sequence alignment of RhoA, Rac1, and Cdc42 subfamily GTPases shows TCL has an extra 18-aa N-terminal extension in comparison to Cdc42. Sequences were aligned using the TCoffee alignment program and the image was produced using Jalview. Only sequences before the GTPase G1 box region are shown. *B,* YFP-tagged TCL and a truncation mutant lacking the first 20 aa (ΔN) were transfected into HeLa cells and visualized for localization using confocal microscopy. *Scale bars* shown in the *lower right corners* are equal to 5 μm. *C,* the percentage of cells displaying a plasma membrane localization *versus* a vesicular pattern was determined for HeLa cells transfected with YFP-tagged TCL and the ΔN mutant in a blind experiment. Greater than 100 cells were counted per coverslip, and *error bars* indicate the standard deviation of three separate coverslips ($p < 0.0002$). Individual data points for each triplicate sample are also indicated.

obvious primary sequence differences between TCL and its closest relatives within the Cdc42 family of GTPases. One obvious region of divergence is the C-terminal hypervariable domains that target Cdc42 family GTPases to different membrane environments; however, we were intrigued by the additional differences in signaling specificity provided by variations in their N termini (17). For example, TC10 contains a 14-amino acid N-terminal extension in comparison to Cdc42, and two short GAG and GPG amino acid sequences within the N terminus help localize TC10 to plasma membrane lipid rafts (18). Another example is provided by the N-terminal polyproline sequences found within the Cdc42 homologue Wrch1. The N-terminal region normally autoinhibits Wrch1, but binding of SH3 domain proteins to the polyproline sequence within the N terminus permits spontaneous binding of GTP and activation of Wrch (19, 20). TCL differs from the other Cdc42-family GTPases in that it possesses a unique N-terminal extension of 18 amino acids in comparison to Cdc42; however, its function has not been investigated.

The results in this paper will show the N terminus plays an important role in TCL localization, and the deletion or mutation of amino acids 17–20 within the N terminus causes the protein to redistribute from predominantly a plasma membrane association to intracellular vesicles. Interestingly, we found that effective GTP loading of TCL also requires the presence of these amino acids, indicating this region allosterically regulates the nucleotide binding pocket. This effect was not recapitulated with the TC10, the closest homologue of TCL. Using this difference, we were able to generate a series of TCL/TC10 chimeras to isolate the region of TCL that coordinates with its N terminus to allosterically regulate nucleotide exchange. Taken together, these results highlight unique attributes of the primary structure of TCL that will aid in further elucidation of its function and provide an important framework to understanding the cellular biochemistry of TCL.

Results

TCL Localization and Activation State Is Dependent Upon Its N Terminus—A sequence alignment of RhoA, Rac1, Cdc42 and close homologues of Cdc42 indicate TCL has a unique 20-amino acid N terminus before the sequence converges on the more conserved GTPase "core" amino acids (Fig. 1*A*) (21, 22). To determine the purpose of this additional sequence, full-length TCL and a deletion mutant removing the first 20 codons (ΔN) were PCR amplified and subcloned into a mammalian expression plasmid to produce YFP-tagged fusions, with the YFP positioned N-terminal to the WT and the ΔN sequences to preserve C-terminal *CAAX* modifications (3, 17, 23). When the expression plasmids were transfected into HeLa cells, YFP-tagged TCL showed a clear peripheral, plasma membrane localization pattern, whereas the ΔN mutant distributed to vesicular compartments (Fig. 1*B*). The redistribution was obvious in blind cell counts, with the ΔN mutant localizing to vesicle structures in about 80% of cells in comparison to full-length TCL (Fig. 1*C*). It should be noted that although a confocal microscope was used for capturing high resolution images of YFP-TCL and TCL mutants to qualitatively evaluate localization, the membrane/vesicle distribution was easily detectable using a simple epifluorescence microscope, and this was routinely used for cell counting experiments (see "Experimental Procedures"). Additionally, human umbilical vein endothelial cells (not shown) were transfected with the TCL and ΔN plasmids as they express significantly higher amounts of endogenous TCL (5). They also displayed a similar localization of TCL

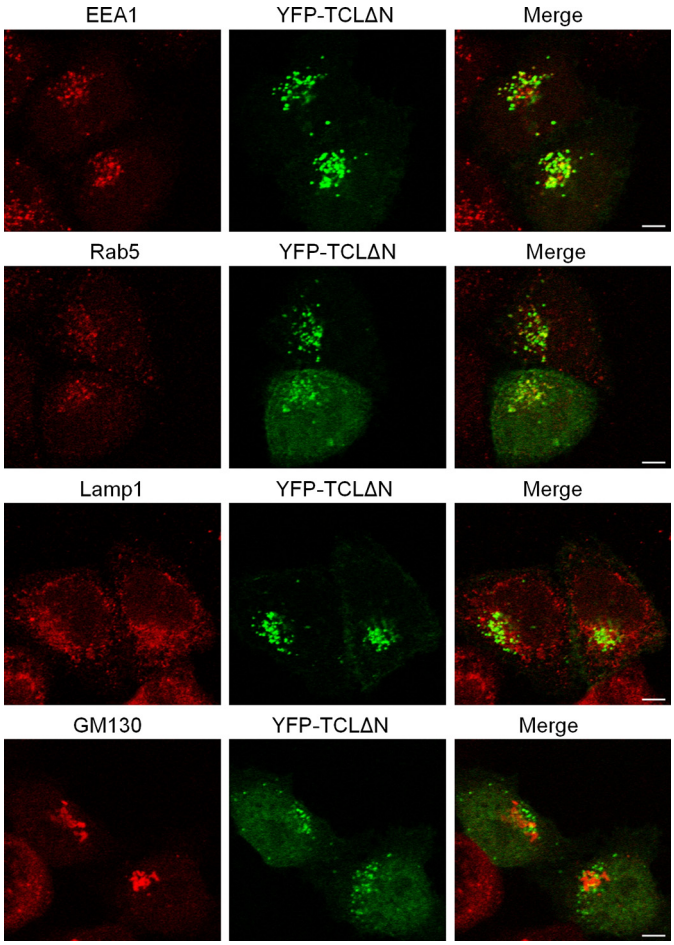

FIGURE 2. **The ΔN mutant of TCL associates with endosomal vesicles.** Plasmid encoding the YFP-tagged ΔN mutant was transfected into HeLa cells. Cells were fixed and co-stained with primary antibodies against the endosomal marker proteins EEA1, Rab5, Lamp1, and GM130 and a rhodamine-conjugated secondary antibody. The cells were visualized using confocal microscopy. *Scale bars* shown in the *lower right corners* of the merged images are equal to 5 μm.

and the ΔN mutant, but HeLa cells were used in subsequent experiments due to their higher transfection efficiencies.

Previous observations regarding both exogenous and endogenous TCL have indicated it primarily localizes to the plasma membrane; however, a fraction of the protein has also been localized to punctate, vesicular structures within cells (4, 6). In particular, GFP-tagged TCL has been previously shown to colocalize with EEA1, Rab4, and Rab5 endosomes in HeLa cells (4). To determine whether the ΔN mutant of TCL localized to similar vesicular compartments as full-length TCL, HeLa cells were transfected with the YFP-TCLΔN construct and co-stained for vesicular/endomembrane markers. Consistent with previous observations, the punctate pattern produced by the ΔN mutant at least partly colocalized with the vesicular markers EEA1 and Rab5 but not the cis-Golgi marker GM-130 and lysosomal marker Lamp1 (Fig. 2). These results show the vesicular patterning produced by the ΔN mutant is likely due to a defect in protein transport to or from the plasma membrane and not due to a re-distribution of TCL to unexpected cellular locations, protein aggregates, or other staining artifacts.

Because cellular re-localization of most GTPases follows GTP loading and activation, we were curious how nucleotide loading influenced TCL localization and if the ΔN re-localization to vesicular compartments was independent of the activation state of the GTPase (3, 17, 24). To test this, YFP-tagged TCL and the ΔN mutant were generated as two different constitutively active point mutants (G30V and Q79L) and a dominant-negative point mutant (T35N) to mimic GTP- and GDP-loaded forms of TCL (2, 25). Regardless of the presence or absence of the N terminus, the G30V and Q79L point mutations localized TCL to the plasma membrane, whereas the T35N dominant-negative mutants were only localized within vesicles in a majority of cells (Fig. 3, *A* and *B*). These results indicate that TCL localization is dependent on its activation state but also suggest the N terminus somehow influences or facilitates the activation of wild-type TCL. Additionally, the results indicate that TCL requires the association of a GAP to become inactivated because the G30V mutation likely disrupts GAP-catalyzed hydrolysis of GTP-loaded GTPases, whereas the Q79L mutation prevents the catalytic activity of the GTPase itself (26).

To further test the hypothesis that the N terminus might regulate TCL activation, a PAK affinity precipitation assay was used to assess whether TCL and the ΔN mutant displayed differences in GTP/GDP loading in cells (27). As an initial control experiment, the G30V and T35N mutants of TCL were used to test assay conditions, and as expected, the G30V mutant bound to GST-PAK, whereas the T35N mutant had minimal interaction (Fig. 3*C*). Lysates from cells expressing TCL and the ΔN mutant (without the G30V and T35N point mutations) were then used in a PAK precipitation assay. The results indicated the ΔN mutant was less GTP-loaded in comparison to full-length TCL, providing corroborating evidence that the N terminus influenced nucleotide loading of TCL, although the mechanism was unclear.

We were interested in determining if there was a direct, causal link between deletion of the TCL N terminus and GTP loading. To investigate this possibility, GST fusion proteins of TCL and the ΔN mutant were generated, along with Cdc42, TC10, and an N-terminal deletion mutant of TC10 (Fig. 4*A*). These proteins were then used in mant-GTP fluorescence-based binding experiments. Initial loading experiments with Cdc42 and TCL indicated that whereas Cdc42 bound mant-GTP in the presence of EDTA and absence of magnesium, TCL loaded with mant-GTP only in the presence of excess magnesium, with slower kinetics and a lower overall increase in total relative fluorescence compared with Cdc42 (Fig. 4*B*). These results were similar to those previously reported for TC10, which also was shown to require excess magnesium to stabilize nucleotide binding (28). Our purified TC10 fusion protein behaved comparably (Fig. 4*C*). More interestingly, however, the deletion of the N terminus of TC10 did not affect its ability to load with mant-GTP, whereas deletion of the TCL N terminus significantly disrupted mant-GTP binding. These results indicate a distinct difference between the influences of the N termini of TCL and TC10 on nucleotide loading, and also potentially explain the cellular effects detected with the TCL ΔN mutant in regard to localization and PAK precipitation experiments.

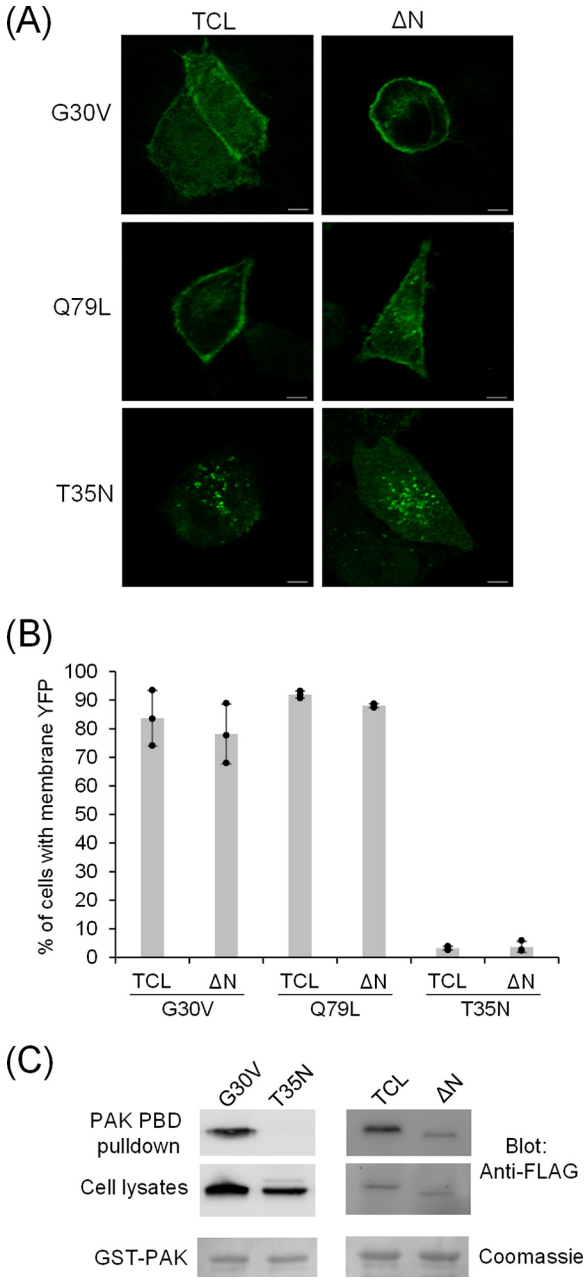

FIGURE 3. **Activation of TCL determines its cellular localization.** *A,* constitutively active (G30V and Q79L) and dominant-negative (T35N) mutants of TCL and the ΔN truncation were produced as YFP-tagged constructs, transfected into HeLa cells, and visualized using confocal microscopy (*scale bars* = 5 μm). *B,* cells were assessed for membrane *versus* vesicular localization of constitutively active and dominant-negative TCL and the ΔN mutant by counting >100 cells per coverslip. *Error bars* indicate the standard deviation determined from the counts of three separate coverslips, and individual data points for each triplicate sample are also indicated. *C,* a PAK precipitation assay was used to compare relative levels of activated TCL in cells. The panels on the *left* display a control experiment to determine relative binding of constitutively active (G30V) and dominant-negative (T35N) TCL with GST-PAK. The panels on the *right* indicate the relative interaction of wild-type TCL and the ΔN mutant with GST-PAK. The *upper blot* shows the relative amount of activated, FLAG-tagged TCL precipitated with GST-PAK, and the *lower blots* show expression of FLAG-tagged proteins in cell lysates and a Coomassie-stained GST-PAK loading control. Results are representative of duplicate experiments.

We explored possible mechanisms to explain why the ΔN mutant displayed differences in mant-GTP loading in comparison to wild-type TCL. One possibility was that pre-bound nucleotide was not as efficiently removed from the ΔN mutant with the concentration of EDTA used in our initial assays, preventing efficient association of mant-GTP. If this was the case, an increased concentration of EDTA would be expected to better remove bound Mg^{2+} from the GTPase, promoting more efficient mant-GTP loading. We therefore tried increasing EDTA concentrations to 1, 3, and 10 mM, with a concurrent increase in $MgCl_2$ to 30 mM to supply a saturating concentration of free Mg^{2+}. The increased concentration of EDTA to 3 (not shown) and 10 mM had no effect on the ΔN mutant; however, it caused full-length TCL to load less efficiently (Fig. 4*D*). These results show that TCL differs from Cdc42 in that TCL likely requires simultaneous coordination of nucleotide and Mg^{2+} to stabilize the bound nucleotide.

We also performed mant-GTP loading experiments with TCL and the ΔN mutant over a longer time course (Fig. 4*E*). In these experiments, the ΔN mutant bound mant-GTP to a level similar to wild-type TCL after about 1 h, indicating the ΔN mutant defect is largely due to slowed nucleotide exchange rather than a complete inability to bind nucleotide. These results also help explain the experimental results involving the constitutively active ΔN mutants in Fig. 3, *A* and *B*, as it implies the ΔN mutant can physically load with GTP in the constitutively active forms leading to membrane association, but the loading is probably occurring at a slowed rate. Additionally, it indicates the amount of precipitated ΔN mutant detected in PAK assays represents the amount of GTP-loaded ΔN mutant and not just a nonspecific background amount, particularly as the T35N mutant of TCL showed exceptionally low background binding (Fig. 3*C*).

Amino Acids 17–20 within the N Terminus of TCL Influence Activation and Localization—A series of progressive N-terminal truncation mutants were generated to pinpoint the specific amino acids involved in altering TCL localization and activation (Fig. 5*A*). HeLa cells transfected with YFP-tagged truncation mutants were visualized and counted to determine plasma membrane or vesicular localization patterns. The first set of truncations deleted 5 amino acids at a time from the N terminus (Δ5, 10, and 15). These truncations had no significant effect on localization (Fig. 5*B*, *left graph*), so progressive single amino acid truncations were made from amino acids 16 to 20 (ΔN). With this set of truncations, the alteration in localization was apparent after deletion of Glu-18 and resembled the ΔN mutant in its vesicular patterning (Fig. 5, *B*, *right graph*, and *C*). All of the truncations were also generated as GST fusion proteins for *in vitro* mant-GTP loading experiments. These results correlated with the localization of TCL, and only the Δ18 and Δ19 mutants had a loading defect similar to the ΔN mutant (Fig. 5, *D* and *E*), indicating that minimally Glu-18 and possibly Lys-19 and -20 are important in TCL plasma membrane localization and nucleotide loading.

For both the localization experiments and for the mant-GTP loading assays, the YFP and GST tags represent larger fusion proteins attached to the N terminus of TCL. To ensure the position of the tags was not contributing to TCL localization and loading defects and to confirm a specific role for amino acids 18–20 in localization and activation of TCL, point mutations were made for the amino acids within this region. We

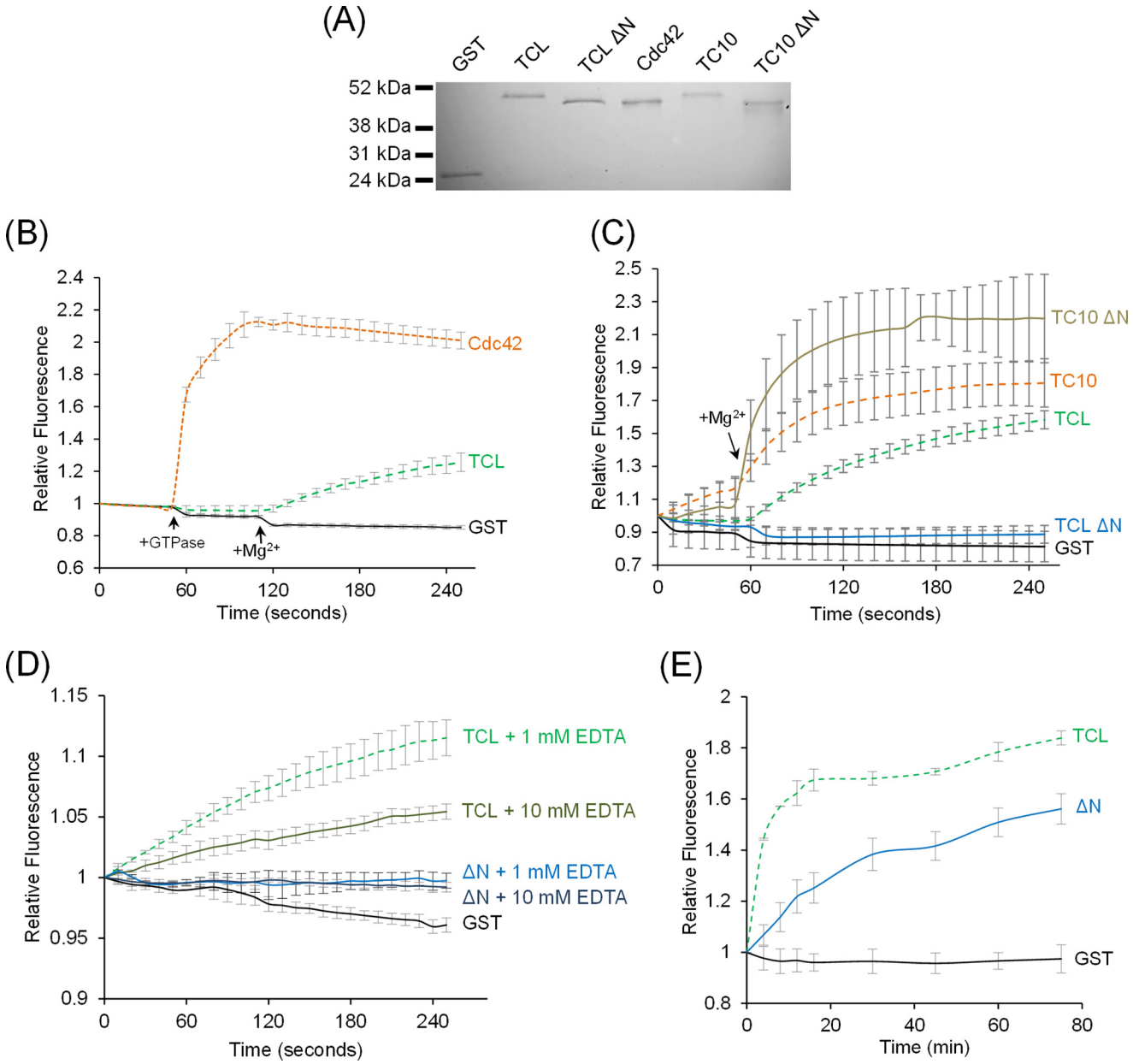

FIGURE 4. **The TCL N terminus is required for efficient nucleotide loading.** *A,* 1 μg of GST fusion proteins was applied to an SDS-PAGE and visualized with Coomassie stain to assess purity and ensure equivalent amounts of protein were added to mant-GTP loading assays. *B,* fluorescence measurements were acquired at 10-s intervals for 1 min using 50 μl of assay buffer (see "Experimental Procedures") containing 0.2 μM mant-GTP. At 1 min, 1 μl of the indicated GTPase was added to the assay buffer to achieve a final concentration of 1 μM and additional readings were taken over the course of 1 min. One μl of concentrated $MgCl_2$ was then added to a final concentration of 10 mM and additional readings were acquired. *C,* a similar assay was performed using GST fusion proteins of TCL, TCLΔN, TC10, and TC10ΔN to assess their loading with mant-GTP. Concentrated $MgCl_2$ was added after 1 min to a final concentration of 10 mM and additional readings were taken. *D,* GST-TCL or the ΔN mutant was added to buffer containing either 1 or 10 mM EDTA prior to the addition of $MgCl_2$ to a final concentration of 30 mM. *E,* a mant-GTP loading experiment was set up as explained under "Experimental Procedures" and monitored over the course of 75 min. For all graphs, *error bars* indicate the standard deviation of normalized fluorescence values for triplicate samples.

chose to divide the amino acids into two groups based on side chain charge. Asp-17 and Glu-18 as well as Lys-19 and Lys-20 were mutated to alanine residues (DE/AA and KK/AA). A poly-alanine mutation spanning the entire sequence was also generated (DEKK/AAAA). The YFP-tagged mutants were then transfected into HeLa cells and assessed for plasma membrane or vesicular localization. Although the KK mutant significantly altered TCL localization in comparison to the wild-type sequence, the DE mutant did not (Fig. 6, *A* and *B*). However, the increased deviation associated with the DE mutants shows the mutation tended to be more difficult to ascribe membrane *versus* vesicular staining in comparison to wild-type TCL. Moreover, the DEKK mutant was the most vesicular of the mutants, indicating Asp-17 and Glu-18 partially contribute to localization along with Lys-19 and Lys-20. Taken together, the results suggest the whole DEKK region is involved with localization of TCL.

We again sought to test whether the localization defect was due to an alteration in activation of TCL using a PAK precipitation assay (Fig. 6*C*). There was decreased association with

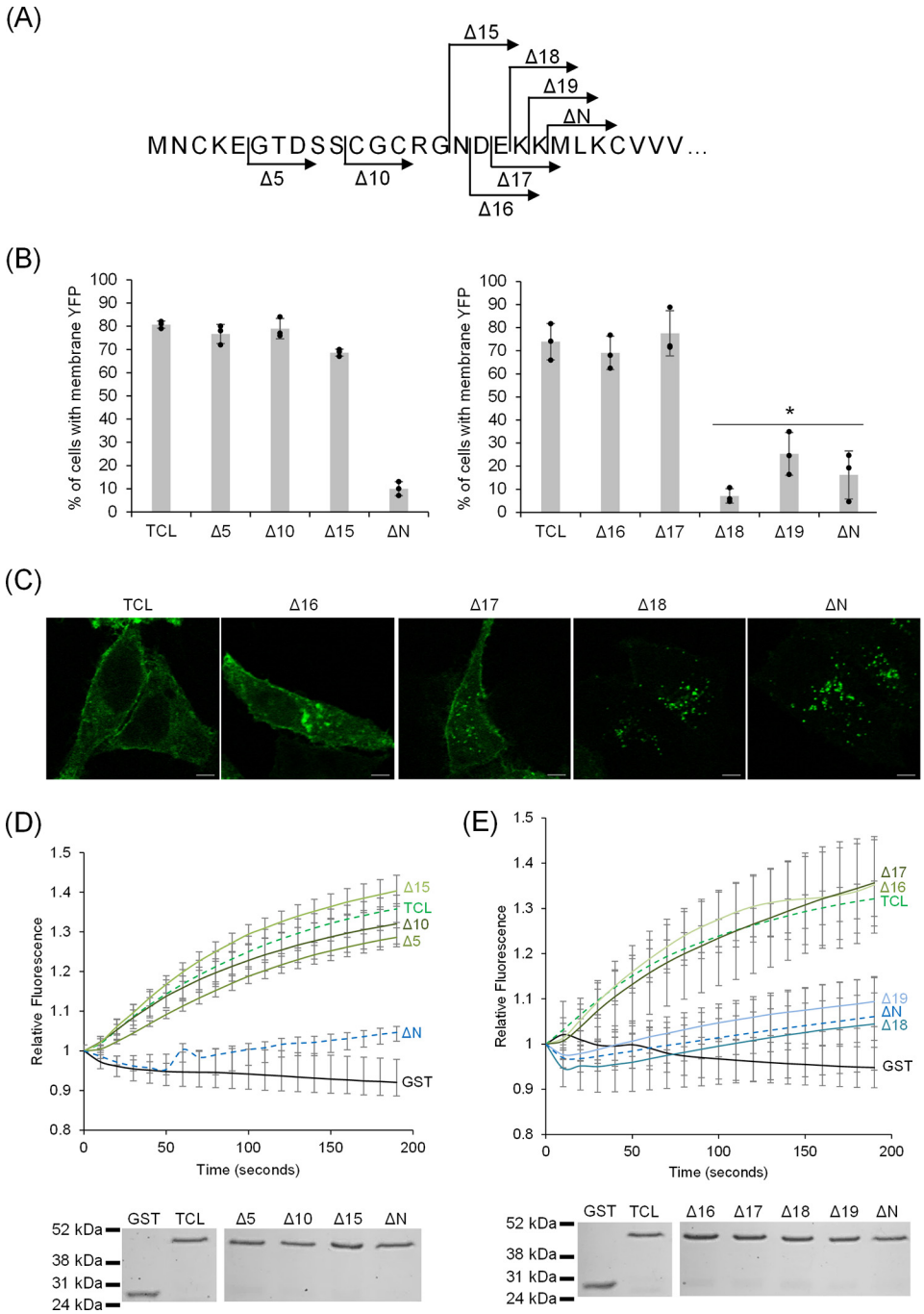

FIGURE 5. **Progressive truncation of the TCL N terminus reveals amino acids 18–20 are essential for plasma membrane localization and GTP loading.** *A,* a diagram of the TCL N-terminal truncation mutants created both as YFP-tagged and GST-tagged constructs. *B,* YFP-tagged TCL truncation mutants were transfected into HeLa cells to determine their subcellular localization. HeLa cells were quantified in a blind experiment, and >100 cells were counted per coverslip to assess membrane *versus* vesicular localization. *Error bars* indicate the standard deviation determined from three separate coverslips, and individual data points for each triplicate sample are indicated. The *asterisk* (*) indicates $p < 0.0025$ for Δ18, Δ19, and ΔN (separately) compared with TCL. *C,* select TCL truncation mutants were visualized using confocal microscopy (*scale bars* = 5 μm). *D* and *E*, *upper panels*: mant-GTP loading assays were conducted as described under "Experimental Procedures" with the indicated TCL truncations. All proteins were used at 1 μM. In these assays, $MgCl_2$ was added to a final concentration of 10 mM to initiate loading. *Error bars* indicate the standard deviation of normalized fluorescence values for triplicate samples. *Lower panels*: 1 μg of GST fusion proteins was applied to SDS-PAGE and visualized with Coomassie stain to assess purity and ensure equivalent amounts of protein were added to mant-GTP loading assays.

GST-PAK for the DEKK and DE mutants, however, the KK mutant showed only a limited decrease in this assay, suggesting GTP exchange is significantly altered for the DEKK and DE mutants in this assay, but not the KK mutant. These same point mutants of TCL were also used to generate GST fusion proteins and tested for nucleotide loading using mant-GTP binding assays (Fig. 6*D*). Notably, all mutants displayed a loading defect; however, mutation of the entire DEKK sequence was required to produce an effect similar to the ΔN mutant. Similar to the PAK precipitation assay, the DE mutant displayed more of a significant loading defect than the KK mutant, but neither was as significant as the DEKK mutant. Together, these results indi-

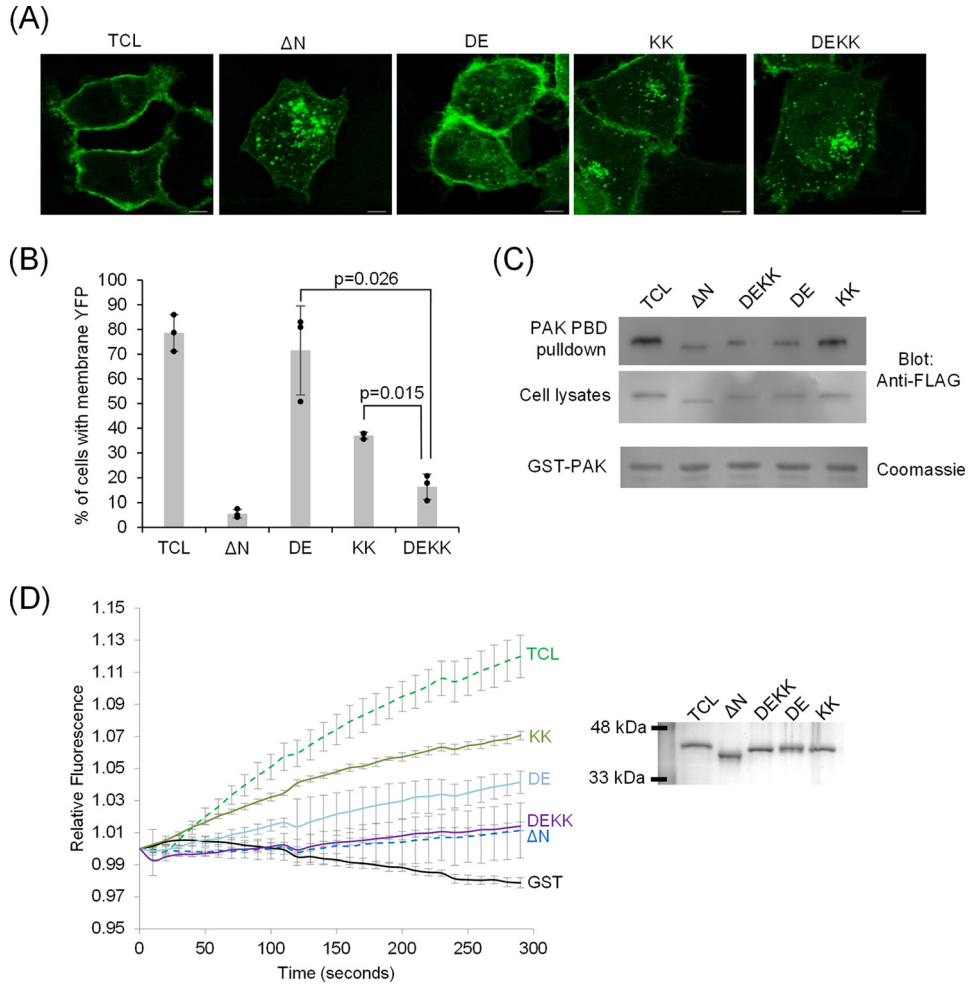

FIGURE 6. **Selectively mutating residues 17–20 of TCL alters localization and nucleotide loading.** *A,* YFP-tagged TCL point mutants $Asp^{17}/Glu^{18} \rightarrow AA$ (DE), $Lys^{19}/Lys^{20} \rightarrow AA$ (KK), and $Asp^{17}/Lys^{20} \rightarrow AAAA$ (DEKK) were transfected into HeLa cells to visualize their subcellular localization using confocal microscopy. *B,* percentage of cells displaying a plasma membrane localization *versus* a vesicular pattern was determined for cells transfected with YFP-tagged TCL point mutants in a blind experiment. *t* test *p* values are provided for the DE and KK mutants in comparison to the DEKK mutant, and individual data points for each triplicate sample are indicated. *C,* a PAK precipitation assay was used to compare activation of TCL point mutants in cells. The *upper blot* shows the relative amounts of activated, FLAG-tagged TCL precipitated with GST-PAK, and the *lower blot* shows expression in cell lysates. Relative amounts of GST-PAK for each sample is indicated with Coomassie stain. Results are representative of duplicate experiments. *D,* mant-GTP loading assays were conducted with the indicated TCL point mutants. All proteins were used at 1 μM, and $MgCl_2$ was added to a final concentration of 10 mM to initiate loading. *Error bars* indicate the standard deviation of normalized fluorescence values for triplicate samples. *Right panel*: 1 μg of GST fusion protein was applied to an SDS-PAGE and visualized with Coomassie stain.

cate amino acids 17–20 of TCL contribute to localization and nucleotide exchange and potentially represent a region facilitating allosteric regulation of the protein; however, amino acids Lys-19 and Lys-20 have a greater effect on localization, whereas amino acids Asp-17 and Glu-18 may contribute more to nucleotide exchange.

Amino Acids Located between Residues 121 and 129 Facilitate N-terminal Regulation of TCL—It was intriguing that deletion of the N terminus from TCL significantly inhibited nucleotide loading, whereas the same deletion had no effect on TC10 (Fig. 3*C*). The results suggested there must be subtle amino acid substitutions within the GTPase core region of TCL (*i.e.* amino acids 21–198) that were responsible for the difference. We were curious if the amino acids could be experimentally identified, and so the sequences for human TCL, TC10, and Cdc42 were aligned to determine sequence differences (Fig. 7*A*) (29). We identified three regions of divergence (designated R1, R2, and R3) as possible sites that could be responsible for the variation between TCL and TC10, and we generated TCL chimeras where the codons within the three regions were swapped with codons from TC10 using a PCR mutagenesis technique (30). A fourth chimera was also generated that swapped all the codons spanning the sequence from R1 through R3 (R1–3). Importantly, all of the chimeras were produced in the context of the ΔN deletion of TCL to identify a region capable of rescuing the loading defect. Three amino acids near the C-terminal end of TCL were not swapped in this analysis.

Because we were looking for a direct alteration of nucleotide loading with the TCL/TC10 chimeras, the proteins were purified as GST fusions and screened for their ability to load with mant-GTP. Our first experiments demonstrated that the R2 chimera allowed the TCL ΔN deletion to bind mant-GTP similar to the TC10 ΔN deletion (Fig. 7*B*). The R1 and R3 regions had no effect in the assay, whereas the R1–3 chimera also had the ability to load with nucleotide. We decided to subdivide the R2 region into additional regions designated a, b, c, and d and

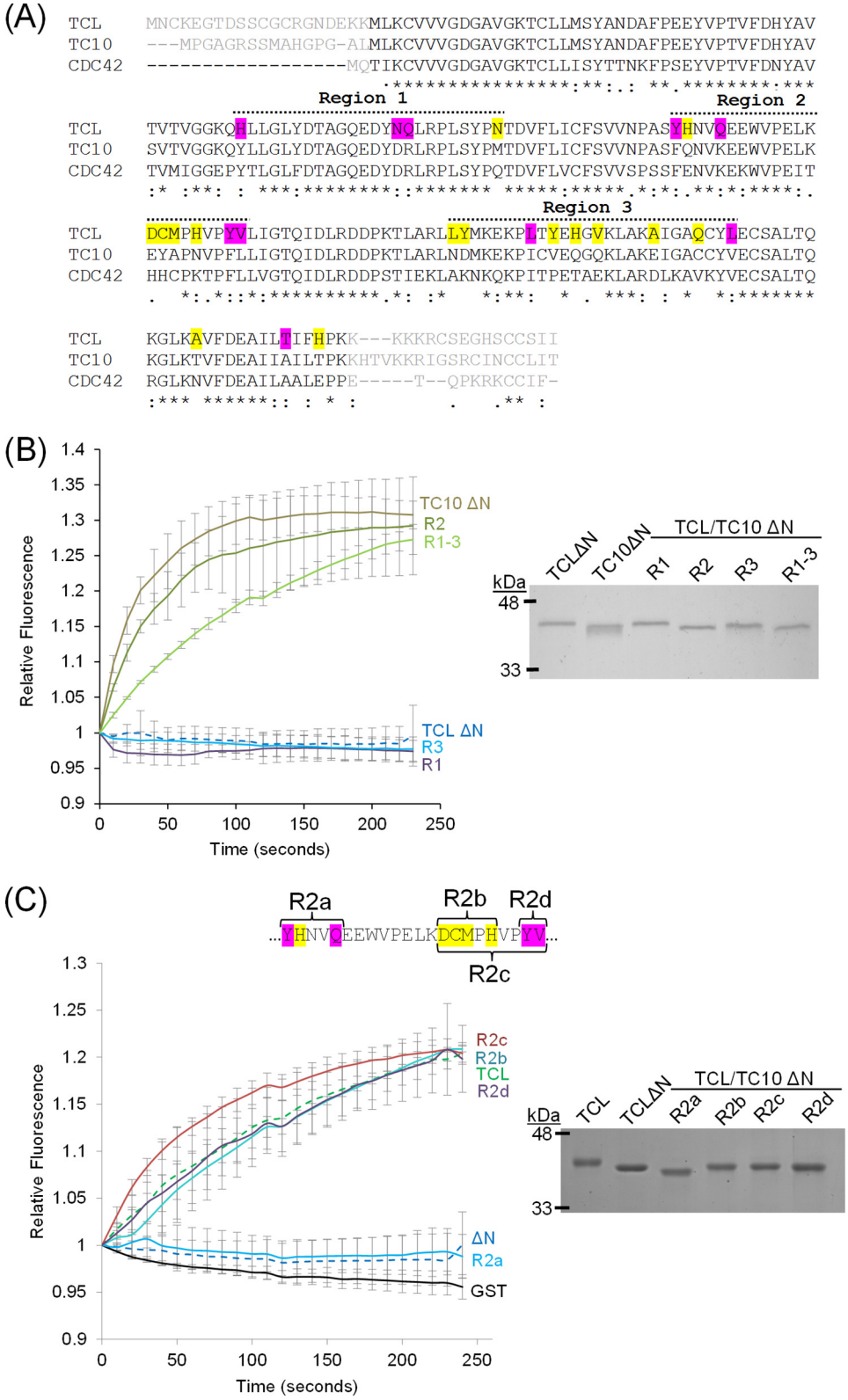

FIGURE 7. **Chimeras of TCL and TC10 reveal a region of TCL that facilitates N-terminal regulation.** *A,* sequences for *H. sapiens* TCL, TC10, and Cdc42 were aligned using CLUSTAL. The N and C termini are in *gray text*, whereas the core GTPase region is indicated in *black*. *Magenta* highlighting within the TCL sequence indicates amino acids that are conserved between TC10 and Cdc42, but not TCL. *Yellow* highlighting indicates amino acids that diverge in all three GTPases. Three regions (regions 1, 2, and 3) of TCL sequence divergence were identified and are specified by *dotted lines above* the TCL sequence. *B*, TCL/TC10 ΔN chimeras were produced by swapping codons for the three regions of TCL identified in *A* with codons from TC10 as described under "Experimental Procedures." GST fusion proteins corresponding to the chimeras were purified and used in a mant-GTP loading assay. $MgCl_2$ was added to a final concentration of 10 mM to initiate loading and fluorescence was measured every 10 s. *Right panel*: 1 μg of GST fusion protein was applied to an SDS-PAGE and visualized with Coomassie stain. *C*, region 2 was further split into four subdivisions (a, b, c, and d) and GST fusion proteins of these TCL/TC10 ΔN chimeras were produced and used in mant-GTP loading assays. For *B* and *C*, *error bars* indicate the standard deviation of normalized fluorescence values for triplicate samples.

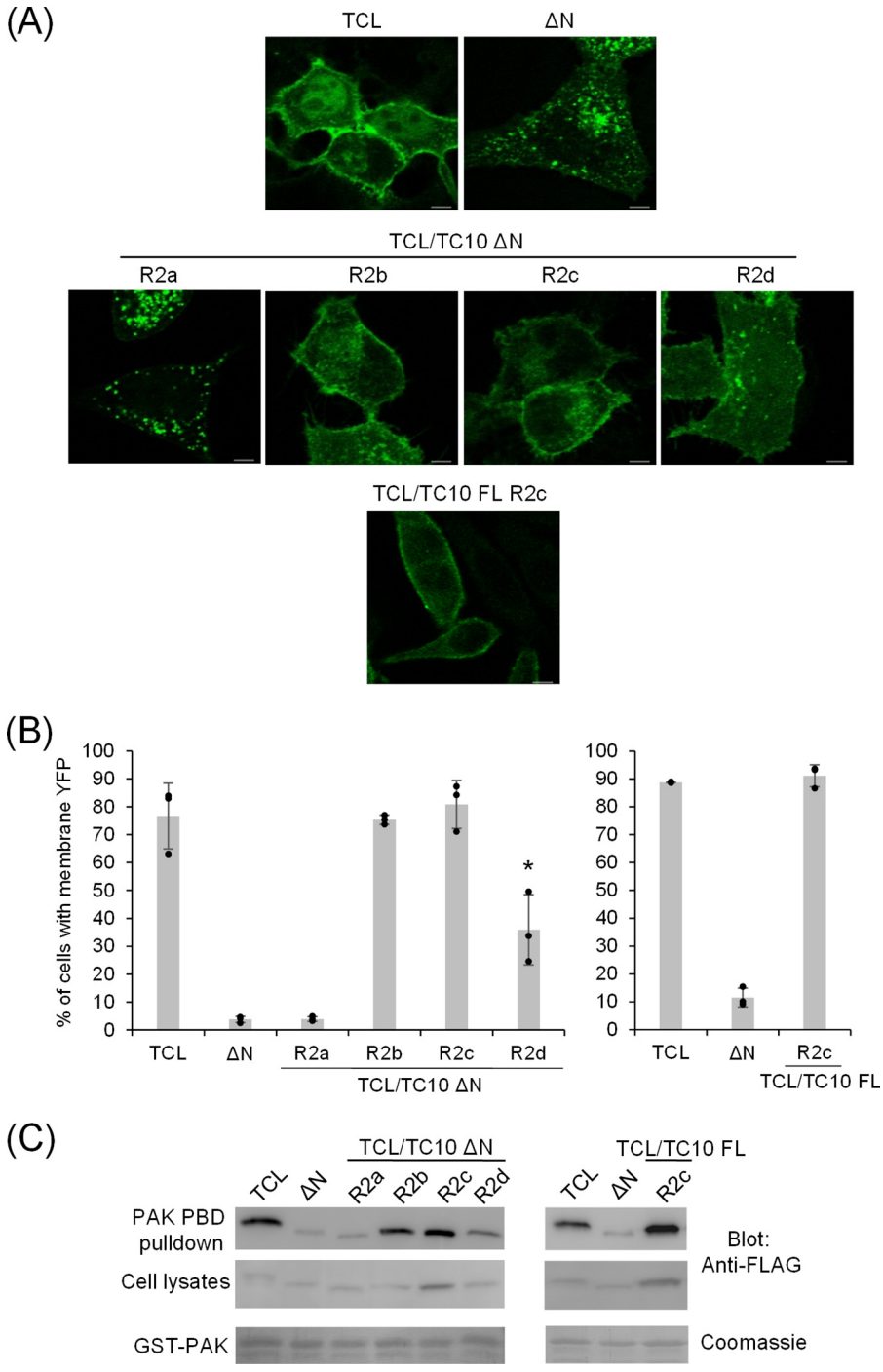

FIGURE 8. **Regions 2b and 2c TCL/TC10 ΔN chimeras are localized and activated similar to wild-type TCL.** *A,* YFP-tagged TCL, the ΔN mutant, and TCL/TC10 ΔN chimeras corresponding to regions 2a, -b, -c, and -d (as specified in Fig. 7*c*) were transfected into HeLa cells and visualized using confocal microscopy. YFP-tagged TCL/TC10 FL (full-length) R2c was used as an additional control. *B,* percent of cells displaying plasma membrane localization *versus* a vesicular pattern was determined for YFP-TCL, the ΔN mutant, and TCL/TC10 ΔN R2 mutants in a blind experiment as indicated in the legend to Fig. 1. The R2d mutant was compared with the R2a and -b, with $p < 0.05$ (*asterisk*). The TCL/TC10 FL R2c mutant was used in an additional control experiment. Individual data points for all triplicate samples are also indicated. *C,* a PAK precipitation assay was used to compare activation of TCL, the ΔN mutant, and TCL/TC10 ΔN R2a, -b, -c, and -d chimeras in cells. A control experiment using TCL/TC10 FL R2c mutant was also performed. The *upper blot* shows the relative amounts of activated, FLAG-tagged TCL precipitated with GST-PAK, and the *lower blot* shows expression in cell lysates. Relative amounts of GST-PAK for each sample is indicated with Coomassie stain. Results are representative of duplicate experiments.

created TCL/TC10 ΔN chimeras with these shorter regions. Fusion proteins of these chimeras identified regions b, c, and d as regions that influence the effect of the N terminus on nucleotide binding of TCL, whereas the chimera of the R2a region had no effect (Fig. 7*C*).

The TCL/TC10 ΔN R2a, -b, -c, and -d chimeras were also tested to see if they influenced membrane localization (Fig. 8, *A* and *B*). The R2b and -c chimeras transitioned TCL/TC10 ΔN from vesicular to membrane localization in comparison the TCL ΔN, whereas the R2a chimera had no effect (Fig. 8, *A* and

B). In these particular experiments, the R2d chimera showed an intermediate effect and was distributed evenly between vesicular and membrane environments, and shows amino acids Tyr-128 and Val-129 have less of a critical influence on nucleotide exchange and localization than the R2b region. As an additional experimental control, an R2c chimera was produced in the context of full-length TCL (TCL/TC10 FL R2c) that retained the N terminus. As expected, this mutant behaved analogous to the wild-type TCL protein in our experiments. Cellular activation of the TCL/TC10 ΔN R2 chimeras was further verified with PAK precipitation assays, and the ΔN R2b and -c chimeras showed enhanced activation in comparison to the TCL ΔN mutant, reaching levels of activation comparable with wild-type TCL (Fig. 8*C*). The R2d mutant was only slightly more active than the ΔN or R2a mutants, mirroring the results obtained with cell counts. The TCL/TC10 FL R2c chimera was also used as an experimental control to ensure this mutant behaved like wild-type TCL. Overall, the results demonstrate amino acids within region R2c allosterically alter the nucleotide binding pocket of TCL so that the GTPase is responsive to the presence of amino acids 17–20.

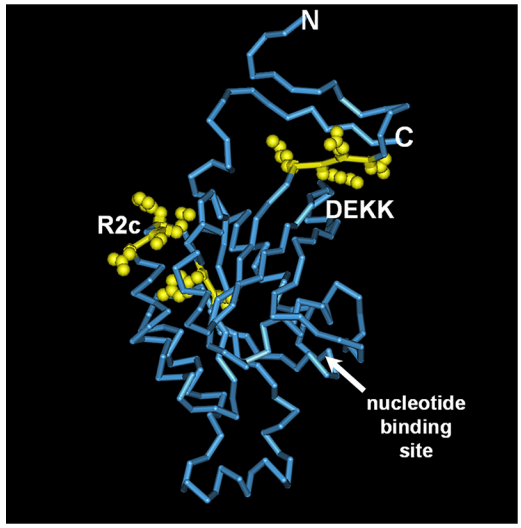

FIGURE 9. **A model of TCL relating the N-terminal DEKK sequence and region 2c.** The structure was produced from the amino acid sequence of TCL using RaptorX. The location of region 2C and Asp^{17}-Lys^{20} are indicated, along with the general location of the nucleotide binding pocket.

Discussion

Amino acids 17–20 within the N terminus and key amino acids spanning from 121 to 129 (R2c) of TCL have an interconnected role in coordinately regulating nucleotide loading and therefore downstream signaling of the GTPase. In this regard, TCL is distinctive in comparison to its closest homologues Cdc42 and TC10 and our results begin to unravel the cellular mechanism of TCL activation that currently lacks a clear, direct exchange process (8). Our results also demonstrate that GDP- and GTP-loaded forms of TCL compartmentalize differently in the cell and suggest the protein shuttles between an endosomal compartment in the GDP-loaded conformation and cellular membrane compartment when the protein is in the GTP-loaded form.

Although it was surprising that the extended N terminus of TCL functioned so differently in comparison to its closest homologue TC10, a better comparison might be made with the more divergent Cdc42 homologue Wrch1/RhoU. For Wrch1, the N terminus acts as an autoinhibitory region, and polyproline sequences within the region facilitate interactions with SH3 domain proteins such as Grb2 that potentially relieve the autoinhibition, allowing spontaneous GTP loading of the GTPase (19, 31). Although similar in terms of being regulated by its N terminus, our current hypothesis is that TCL may likely behave in an opposite manner, with the N terminus, particularly the DEKK sequence, binding a regulatory factor or acting to govern posttranslational modifications that inhibit nucleotide exchange. It is also possible that the DEKK sequence modulates activity when the protein is brought into contact with different membrane environments, and this could partly explain the behavior of the separate DE and KK mutants in our experiments (23, 32, 33). Although both independently influenced nucleotide loading to varying degrees, amino acids Lys-19 and Lys-20 could be more involved with facilitating recruitment of TCL to the plasma membrane through interactions with negatively charged phospholipids and less directly involved in nucleotide loading (32, 33). Additional interactions at the plasma membrane could then allow amino acids Asp-17 and Glu-18 to facilitate nucleotide exchange.

Because TCL nucleotide binding is uniquely influenced by its N terminus, it was reasonable to expect specific amino acid variations to be required within the GTPase core so nucleotide exchange would be responsive to the N terminus. In our experiments, a relatively short sequence controlled this effect, and swapping amino acids 121–125 of TCL with amino acids from TC10 was sufficient to cause the ΔN mutant of TCL to behave like the wild-type protein both in terms of nucleotide loading and cellular localization. However, the Y128F/V129L chimera (*i.e.* R2d) also influenced the loading of TCL, suggesting the whole region from 121 to 129 (*i.e.* R2c) regulates the responsiveness of TCL to the presence of its N terminus. Like the DEKK sequence, this region could also operate as a site for interaction with regulatory proteins or post-translational modification.

Fig. 9 provides a hypothetical structure of TCL generated using RaptorX and shows the location of the N-terminal DEKK sequence in relationship to the R2c region (34). Based upon this model and its similarities to the crystal structure of TC10, the DEKK sequence and R2c region are expected to be about 20 Å apart from each other, with none of the residues contacting a bound magnesium ion or guanine nucleotide (35). The two regions are therefore unlikely to directly contact each other or bound cofactors to coordinate nucleotide exchange; although, it is conceivable the two regions are brought into intermolecular proximity and direct contact through dimer- or multimerization of TCL similar to what has been reported for Ras and other Rho GTPases (36, 37). Instead, we believe the two regions function together to allosterically attenuate the nucleotide binding pocket, rendering TCL sensitive to nucleotide exchange through molecular alterations and modifications in one or both regions. Nucleotide exchange could then be promoted through post-translational modifications or protein/protein interactions involving either the N terminus or the R2c region, supporting a non-GEF based exchange mechanism for TCL. The spatial orientation of the DEKK sequence

TABLE 1
Forward and reverse primers for full-length and truncation sequences

Name	Direction	Sequence (restriction enzyme sites in bold)
TCL	Forward	5′-cattgctagc**aagctt**aactgcaaagagggaactgacagcagc-3′
ΔN		5′-atcggctgactt**aagctt**atgttgaagtgtgtggtggtg-3′
Δ5		5′-cattgctagc**aagctt**ggaactgacagcagctgcggc-3′
Δ10		5′-cattgctagc**aagctt**tgcggctgcaggggcaacgac-3′
Δ15		5′-cattgctagc**aagctt**aacgacgagaagaagatgttg-3′
Δ16		5′-cattgctagc**aagctt**gacgagaagaagatgttgaagtgtgtggtg-3′
Δ17		5′-cattgctagc**aagctt**gagaagaagatgttgaagtgtgtggtggtg-3′
Δ18		5′-cattgctagc**aagctt**aagaagatgttgaagtgtgtggtggtgggg-3′
Δ19		5′-cattgctagc**aagctt**aagatgttgaagtgtgtggtggtgggggac-3′
TC10		5′-cattgctagc**aagctt**atgcccggagccggccgcagc-3′
TC10ΔN		5′-cattgctagc**aagctt**atgctcaagtgcgtggtggtcggc-3′
Cdc42		5′-atcggctgactt**aagctt**atgcagacaattaagtgtgtt-3′
TCL	Reverse	5′-gcaacgtcga**gcggccgc**tcagataattgaacagcagct-3′
TCLΔ198		5′-atcggctgactt**gcggccgc**tcacttggggtggaaaatggtgag-3′
TC10Δ193		5′-atcggctgactt**gcggccgc**tcatctttttttacagtgtgtttc-3′
Cdc42Δ178		5′-atcggctgactt**gcggccgc**tcactccagggcagccaatattgc-3′

and R2c region to the same surface as the C terminus is also intriguing, and could promote simultaneous interaction of all three regions of TCL at various cellular membranes.

At the cellular level, the distribution of TCL and its correlation with TCL activation indicate GTP loading occurs at or near the plasma membrane and facilitates stable localization to this environment. Deactivation through hydrolysis of GTP would then result in relocalization to the vesicular/endomembrane system. Although this study has focused on the intramolecular regulation of TCL, it will be interesting to study how the N terminus and amino acids 121–129 affect previously studied biological roles of TCL, particularly in regard to activation events involved in endosome sorting and focal adhesion dynamics (4, 16). We are particularly interested in how the results for TCL parallel the localization of Ras isoforms. Localization of Ras proteins is largely regulated by a permanent farnesylation modification and labile palmitoylation modifications that cause redistribution of Ras to the recycling endosomes and the plasma membrane (33, 38–41). Additionally, GTP loading of Ras correlates with a longer plasma membrane association (42). Depalmitoylation of Ras facilitates its localization to the Golgi membrane where it is re-palmitoylated and cycled back to the plasma membrane (40, 43). A similar mechanism could be at play for localization of TCL. This would be contrary to previous studies suggesting TCL is not palmitoylated; however, it is possible the modification is transient and rapidly hydrolyzed, causing the detection of palmitoylated TCL to be more difficult (40, 44). If this were the case, then TCL palmitoylation would possibly modulate GTP loading either by directly altering nucleotide loading or by bringing TCL to a favorable membrane environment for nucleotide exchange to occur.

Overall, our results have uncovered novel aspects related to TCL nucleotide exchange, and identified two sequences that work in tandem to regulate the protein. More work will need to be done to identify how these sequences are modulated in a biological context, but they may point to a direction for the development of targeted drug-design against TCL with the goal of disrupting its function in angiogenesis and other potential disease states. Identifying amino acids 121–129 as allosterically regulating the nucleotide binding pocket may be particularly useful in this regard, as they occur within a comparatively structured portion of TCL, and may be more amenable to targeted drug design (45).

Experimental Procedures

Reagents and Antibodies—M2 mouse anti-FLAG (Sigma), mouse monoclonal anti-LAMP1 (anti-CD107) and mouse monoclonal anti-GM130 (BD Biosciences), rabbit monoclonal anti-EEA1 and rabbit monoclonal anti-Rab5 (Cell Signaling) were used. Secondary antibodies used were goat anti-mouse HRP, goat anti-mouse rhodamine, and goat anti-rabbit rhodamine (Sigma). Mant-GTP (Molecular Probes) was used to detect GTPase nucleotide binding.

Expression Constructs—Plasmids carrying cDNA for *Homo sapiens* TCL (CDS of accession NM020663), TC10 (CDS of accession AF498976), Cdc42 (CDS of accession NM001791), TCL G30V, and TCL T35N were gifts from D. Billadeau (Mayo Clinic, Rochester, MN). Full-length and truncated cDNA fragments were amplified using Phusion polymerase (New England Biolabs) according to the manufacturer's directions. Forward and reverse primers encoded compatible restriction enzyme sites (HindIII and NotI) for insertion into expression plasmids (see Table 1). Fragments were subcloned into either a modified form of pCI (Promega) designated pCI2.F.YFP, which fuses FLAG and YFP tags at the N-terminal end of inserted sequences, or a pGEX plasmid to produce GST fusion proteins. To improve the yield of GST-tagged TCL, TC10, and Cdc42, codons for the unstructured C-terminal tail (aa 198–214 for TCL, 193–213 for TC10, and 178–191 for Cdc42) were removed as previously described (35). GST-tagged TCL and the ΔN mutant were also produced with an intact C-terminal tail; however, the presence of the C-terminal tail did not alter nucleotide loading in mant-GTP loading experiments.

Pfu polymerase (Agilent), along with appropriate forward and complementary reverse primers (Table 2), was used to generate various point mutants and shorter TCL/TC10 chimeras (R2a, -b, and -d), using standard mutagenesis protocols. Longer chimeras of TCL and TC10 were generated in a two-step mutagenesis procedure (30). Phusion polymerase was used to PCR amplify various regions of TC10 using primers that carried flanking TCL sequence (Table 3). The amplified TC10 sequences were then purified using a silica resin-based PCR purification procedure and used directly in mutagenesis reactions to replace TCL codons with TC10 codons. In all cases, purified plasmids were submitted for DNA sequencing to verify the product.

TABLE 2
Forward primers for standard mutagenesis

Name	Forward primer sequence (mutated nucleotides capitalized)
DE/AA	5′-agctgcggctgcaggggcaacgCcgCgaagaagatgttgaagtgtgtg-3′
KK/AA	5′-ggctgcaggggcaacgacgagGCgGCgatgttgaagtgtgtggtggtg-3′
DEKK/AAAA	5′-gcagctgcggctgcaggggcaacgCcgCgGCgGCgatgttgaagtgtgtggtggtggg-3′
TCL/TC10 R2a	5′-tctgtcgtaaaccctgcctcttTccaGaatgtcAaggaggaatgggtccccgagctc-3′
TCL/TC10 R2b	5′-gaatgggtccccgagctcaaggaGtAcGCgcctAacgtgccttatgtcctcataggg-3′
TCL/TC10 R2d	5′-gactgcatgcctcacgtgccttTtCtcctcatagggacccagattgat-3′

Cell Culture and Transfection—HeLa cells were cultured in RPMI 1640 medium supplemented with 5% (v/v) fetal bovine serum and 5% (v/v) bovine calf serum. Cells were trypsinized and replated 1 day prior to transfection. For microscopy experiments, sterile glass coverslips were added to 35-mm culture dishes prior to seeding with 0.7×10^6 cells. For PAK assays, 60-mm dishes were seeded with 1.3×10^6 cells. Lipofectamine 3000 was routinely used for transfections (Invitrogen). Cells were incubated with transfection complexes for 20–24 h before using in experiments.

Expression and Purification of GST Fusion Proteins—Fusion proteins were expressed in *Escherichia coli* BL21(DE3) cells in LB (Luria-Bertani) broth containing 100 μg/ml of ampicillin essentially as previously described with some minor alterations (46). For purification, 2 ml of a starter culture (grown overnight) was used to inoculate 100 ml of LB containing ampicillin. Cultures were then incubated in a shaker for 2 h at room temperature (22 °C). Isopropyl β-D-thiogalactopyranoside was added to 75 μM final concentration, and cultures were incubated with shaking at 18 °C overnight. Cultures were centrifuged at 4 °C for 5 min at 2,000 $\times$ *g* and the supernatant was removed, and the remaining steps were conducted on ice. Five ml of a lysis buffer containing 20 mM Tris, pH 7.5, 50 mM NaCl, 5.0 mM $MgCl_2$, 2 mM DTT, and 10 μM GDP was added to each pellet. Pellets were resuspended and lysed on ice using a sonicator with a microtip and a total of six ~300 joule bursts of 15 s each. Cell lysates were centrifuged at 4 °C for 5 min at 20,000 $\times$ *g* and the supernatant was added to 0.5 ml of packed GSH resin. Bacterial lysates and resin were rotated at 4 °C for 30 min. After incubation, tubes containing the lysate and resin were centrifuged at 4 °C for 1 min at 200 $\times$ *g*. The supernatant was removed and the resin was resuspended in 10 ml of wash buffer containing 20 mM Tris, pH 7.5, 50 mM NaCl, and 0.5 mM $MgCl_2$. The wash step was repeated, and after removing the second wash solution, 500 μl of elution buffer (wash buffer with 15 mM glutathione) was added and mixed with the resin. To maintain optimal protein activity, glycerol was added to 10% (v/v) final concentration immediately after purification, the proteins were aliquoted into several tubes on ice, snap frozen in liquid nitrogen, and stored at −80 °C. Protein concentrations were determined using gel densitometry of appropriate bands on Coomassie Blue-stained SDS-PAGE gels, using BSA as a protein standard. Purification typically yielded protein concentrations of 10–30 μM.

Immunocytochemistry—For all fluorescence microscopy experiments, media was removed from cells grown and transfected on 35-mm dishes containing coverslips. The cells were washed once with 400 μl of PBS and fixed with 4% (v/v) paraformaldehyde in PBS for 15 min. For colocalization experiments requiring antibody staining, coverslips were rinsed three times with PBS for 5 min each and then incubated in blocking buffer (1× PBS, 0.3% Triton X-100, 5% normal goat serum) for 1 h. Coverslips were incubated overnight with primary antibodies in dilution buffer (1× PBS, 1% BSA, and 0.3% Triton X-100) at 4 °C. Primary antibodies were used at the following dilutions: EEA1, CD107, and GM130 were at a 1:50 dilution and Rab5 at 1:100. Coverslips were washed three times with PBS, and primary antibodies were detected by incubating the coverslips for 2 h with a rhodamine-conjugated anti-mouse or anti-rabbit antibody (1:250) in dilution buffer. For all fluorescence microcopy experiments, coverslips were washed three times with PBS, briefly immersed in sterile water, and dried for 30 min at 37 °C. Dried coverslips were mounted onto slides using ProLong Gold AntiFade Reagent (Life Technologies).

Fluorescence Microscopy—Images of fixed cells were captured at the University of North Dakota (Grand Forks, ND) microscopy core facility using a Zeiss LSM 510 Meta microscope equipped with a ×100 oil Plan-Fluor objective with a 1.45 numerical aperture. Images were assembled using Zen 2012 blue edition software.

For quantitative analysis of membrane and vesicular localization, three individual coverslips were transfected for a particular plasmid/construct. All coverslips within an experiment were then randomized, given a number, and cells were counted in a blind experiment. Cells were viewed under an Olympus BH2 fluorescence microscope using a ×40 objective (NA = 0.70) and at least 100 cells were randomly counted per coverslip. Cells with bright, plasma membrane-associated YFP fluorescence but less vesicular fluorescence were counted as having membrane localization, cells with more obvious vesicular/intracellular fluorescence were marked as vesicular. Cells displaying an extremely bright fluorescence were not counted (~5% of cells).

PAK Affinity Precipitation Assay—Activated TCL was detected in cells using the standard GST-PAK affinity precipitation assay with some modifications (27, 47). For each sample in an experiment, 20 μg of GST fusion protein containing the GTPase binding region of PAK was bound to 30 μl of GSH-agarose slurry in a 1-ml volume of lysis buffer (20 mM Tris, pH 7.5, 50 mM NaCl, 1 mM EDTA, 10 mM $MgCl_2$, 3% glycerol, 0.1% Nonidet P-40, 1 mM DTT and protease inhibitor mixture) at 4 °C for 30 min. The resin was centrifuged, the supernatant was aspirated and washed with an additional 1 ml of lysis buffer. The wash was again removed from the resin and 500 μl of lysis buffer was added back to each tube. Transfected cells on 60-mm culture plates were washed once with 1 ml of ice-cold PBS, and lysed with 700 μl of lysis buffer. Cells were collected by scraping, the lysate was clarified by centrifugation at 12,000 $\times$ *g* for 1 min at 4 °C, and 500 μl of the resulting supernatant was added to the tubes containing the GST-PAK/GSH-agarose complex.

TABLE 3
Forward and reverse primers for two-step mutagenesis

Name	Direction	Sequence (TCL sequence capitalized, TC10 lowercase)
TCL/TC10 R1	Forward	5′-ACTGTGACTGTGGGAGGCAAGCAAtacctcctaggactctatgacacg-3′
	Reverse	5′-AGAGAAGCAGATCAAAAACACATCCGTcattgggtaagataaaggcctcag-3′
TCL/TC10 R2	Forward	5′- TGCTTCTCTGTCGTAAACCCTGCCTCTtttcaaaatgtgaaagaggagtgg-3′
	Reverse	5′-ACGGAGATCAATCTGGGTCCCTATGAGtaaaaagggtacatttggtgcgta-3′
TCL/TC10 R3	Forward	5′-CGTGATGACCCAAAAACCTTGGCCCGTTTGaatgatatgaaagaaaaacct-3′
	Reverse	5′-GAGACCTTTCTGAGTCAGAGCTGAACATTCcacatagcagcatgctcctat-3′
TCL/TC10 R2c	Forward	5′-CCTGCCTCTTACCACAATGTCCAGgaggagtgggtaccggaactt-3′
	Reverse	5′-GAGAGGTTTCTCTTTCATATACAGcagtcttgctaaagttttggg-3′

The lysate and resin were mixed for 15 min at 4 °C before pelleting the resin by centrifugation, aspirating the supernatant, and washing the resin with 1 ml of wash buffer (20 mM Tris, pH 7.5, 50 mM NaCl, 10 mM $MgCl_2$, 0.1% Nonidet P-40). The pelleting and washing steps were repeated two more times, after which all wash buffer was removed before adding 20 μl of SDS-PAGE loading buffer and boiling for 5 min. The samples were applied to a 10% SDS-PAGE gel and analyzed by immunoblotting.

Western Blotting—Proteins were separated by SDS-PAGE, transferred onto PVDF membrane, and incubated with the primary antibody in blocking buffer overnight. Membrane was washed in TBST (TBS + 0.1% Tween 20) and incubated with the appropriate HRP-conjugated secondary antibody in TBST for 40 min before blot development.

Mant-GTP Loading Assays—Unless specified otherwise, binding assays were conducted using 1 μM GTPase protein in a buffer containing 20 mM Tris, pH 7.5, 50 mM NaCl, 0.5 mM EDTA, and 0.2 μM mant-GTP. Fluorescence readings were taken in 10-s intervals using the UV module (excitation = 365 nm, emission = 410–50 nm) equipped with a microtube adaptor of a GloMax-Multi Jr. single tube multimode reader (Promega) before adding $MgCl_2$ to a final concentration of 10 mM. Measurements were taken every 10 s for about 3 min after addition of $MgCl_2$. All assays were performed in triplicate and fluorescence values were normalized to the initial reading for each sample.

Statistical Analysis—Data are represented as mean ± S.D. Where indicated, comparisons between data sets were made with a two-tailed, unpaired, unequal variance *t* test.

Author Contributions—M. J. H. conceived and coordinated the study, performed experiments throughout, and wrote the paper. K. L. A. performed experiments in Figs. 1 and 3–5 and wrote the paper. R. R. F. designed, performed, and analyzed confocal images throughout and mant-GTP experiments shown in Figs. 6 and 7. S. S. R. performed and analyzed the experiments shown in Fig. 7. B. R. T. performed and analyzed cell count experiments in Figs. 6 and 8. All authors reviewed the results and approved the final version of the manuscript.

Acknowledgments—We are grateful to Dr. Dan Billadeau (Mayo Clinic, Rochester, MN) for providing the pCI2.F.YFP and pGEX constructs, as well as constitutively active and dominant-negative TCL mutants, Dr. Bryon Grove and Sarah Abrahamson (UND, Grand Forks, ND) for their assistance with the confocal microscopy, and Dr. Holly LaFerriere for editorial comments. We also acknowledge use of the Edward C. Carlson Imaging and Image Analysis Core Facility, which is supported in part by an Institutional Development Award (IDeA) from the National Institute of General Medical Sciences, National Institutes of Health Grant 1P30GM103329.

References

1. Vignal, E., De Toledo, M., Comunale, F., Ladopoulou, A., Gauthier-Rouvière, C., Blangy, A., and Fort, P. (2000) Characterization of TCL, a new GTPase of the rho family related to TC10 andCcdc42. *J. Biol. Chem.* **275,** 36457–36464
2. Aspenström, P., Fransson, A., and Saras, J. (2004) Rho GTPases have diverse effects on the organization of the actin filament system. *Biochem. J.* **377,** 327–337
3. Ridley, A. J. (2015) Rho GTPase signalling in cell migration. *Curr. Opin. Cell Biol.* **36,** 103–112
4. de Toledo, M., Senic-Matuglia, F., Salamero, J., Uze, G., Comunale, F., Fort, P., and Blangy, A. (2003) The GTP/GDP cycling of rho GTPase TCL is an essential regulator of the early endocytic pathway. *Mol. Biol. Cell.* **14,** 4846–4856
5. Yuan, L., Sacharidou, A., Stratman, A. N., Le Bras, A., Zwiers, P. J., Spokes, K., Bhasin, M., Shih, S.-C., Nagy, J. A., Molema, G., Aird, W. C., Davis, G. E., and Oettgen, P. (2011) RhoJ is an endothelial cell-restricted Rho GTPase that mediates vascular morphogenesis and is regulated by the transcription factor ERG. *Blood* **118,** 1145–1153
6. Kaur, S., Leszczynska, K., Abraham, S., Scarcia, M., Hiltbrunner, S., Marshall, C. J., Mavria, G., Bicknell, R., and Heath, V. L. (2011) RhoJ/TCL regulates endothelial motility and tube formation and modulates actomyosin contractility and focal adhesion numbers. *Arterioscler. Thromb. Vasc. Biol.* **31,** 657–664
7. Takase, H., Matsumoto, K., Yamadera, R., Kubota, Y., Otsu, A., Suzuki, R., Ishitobi, H., Mochizuki, H., Kojima, T., Takano, S., Uchida, K., Takahashi, S., and Ema, M. (2012) Genome-wide identification of endothelial cell-enriched genes in the mouse embryo. *Blood* **120,** 914–923
8. Leszczynska, K., Kaur, S., Wilson, E., Bicknell, R., and Heath, V. L. (2011) The role of RhoJ in endothelial cell biology and angiogenesis. *Biochem. Soc. Trans.* **39,** 1606–1611
9. Kusuhara, S., Fukushima, Y., Fukuhara, S., Jakt, L. M., Okada, M., Shimizu, Y., Hata, M., Nishida, K., Negi, A., Hirashima, M., Mochizuki, N., Nishikawa, S., and Uemura, A. (2012) Arhgef15 promotes retinal angiogenesis by mediating VEGF-induced Cdc42 activation and potentiating RhoJ inactivation in endothelial cells. *PLoS ONE* **7,** e45858
10. Kim, C., Yang, H., Fukushima, Y., Saw, P. E., Lee, J., Park, J.-S., Park, I., Jung, J., Kataoka, H., Lee, D., Heo, W. D., Kim, I., Jon, S., Adams, R. H., Nishikawa, S., Uemura, A., and Koh, G. Y. (2014) Vascular RhoJ is an effective and selective target for tumor angiogenesis and vascular disruption. *Cancer Cell* **25,** 102–117
11. Ho, H., Soto Hopkin, A., Kapadia, R., Vasudeva, P., Schilling, J., and Ganesan, A. K. (2013) RhoJ modulates melanoma invasion by altering actin cytoskeletal dynamics. *Pigment Cell Melanoma Res.* **26,** 218–225
12. Ho, H., Aruri, J., Kapadia, R., Mehr, H., White, M. A., and Ganesan, A. K. (2012) RhoJ regulates melanoma chemoresistance by suppressing pathways that sense DNA damage. *Cancer Res.* **72,** 5516–5528
13. Hou, A., Toh, L. X., Gan, K. H., Lee, K. J., Manser, E., and Tong, L. (2013) Rho GTPases and regulation of cell migration and polarization in human corneal epithelial cells. *PLoS ONE* **8,** e77107
14. Ruusala, A., and Aspenström, P. (2004) Isolation and characterisation of DOCK8, a member of the DOCK180-related regulators of cell morphology. *FEBS Lett.* **572,** 159–166
15. Jaiswal, M., Dvorsky, R., and Ahmadian, M. R. (2013) Deciphering the molecular and functional basis of Dbl family proteins: a novel systematic

approach toward classification of selective activation of the Rho family proteins. *J. Biol. Chem.* **288,** 4486–4500
16. Wilson, E., Leszczynska, K., Poulter, N. S., Edelmann, F., Salisbury, V. A., Noy, P. J., Bacon, A., Rappoport, J. Z., Heath, J. K., Bicknell, R., and Heath, V. L. (2014) RhoJ interacts with the GIT-PIX complex and regulates focal adhesion disassembly. *J. Cell Sci.* **127,** 3039–3051
17. Wennerberg, K., and Der, C. J. (2004) Rho-family GTPases: it's not only Rac and Rho (and I like it). *J. Cell Sci.* **117,** 1301–1312
18. Chunqiu Hou, J., and Pessin, J. E. (2003) Lipid Raft targeting of the TC10 amino terminal domain is responsible for disruption of adipocyte cortical actin. *Mol. Biol. Cell.* **14,** 3578–3591
19. Shutes, A., Berzat, A. C., Cox, A. D., and Der, C. J. (2004) Atypical mechanism of regulation of the Wrch-1 Rho family small GTPase. *Curr. Biol.* **14,** 2052–2056
20. Shutes, A., Berzat, A. C., Chenette, E. J., Cox, A. D., and Der, C. J. (2006) Biochemical analyses of the Wrch atypical Rho family GTPases. *Methods Enzymol.* **406,** 11–26
21. Waterhouse, A. M., Procter, J. B., Martin, D. M., Clamp, M., and Barton, G. J. (2009) Jalview Version 2: a multiple sequence alignment editor and analysis workbench. *Bioinformatics* **25,** 1189–1191
22. Notredame, C., Higgins, D. G., and Heringa, J. (2000) T-Coffee: a novel method for fast and accurate multiple sequence alignment. *J. Mol. Biol.* **302,** 205–217
23. Ridley, A. J. (2006) Rho GTPases and actin dynamics in membrane protrusions and vesicle trafficking. *Trends Cell Biol.* **16,** 522–529
24. Braun, A. C., and Olayioye, M. A. (2015) Rho regulation: DLC proteins in space and time. *Cell. Signal.* **27,** 1643–1651
25. Hall, A. (1998) Rho GTPases and the actin cytoskeleton. *Science* **279,** 509–514
26. Prior, I. A., Lewis, P. D., and Mattos, C. (2012) A comprehensive survey of Ras mutations in cancer. *Cancer Res.* **72,** 2457–2467
27. Benard, V., and Bokoch, G. M. (2002) Assay of Cdc42, Rac, and Rho GTPase activation by affinity methods. *Methods Enzymol.* **345,** 349–359
28. Bridges, D., Chang, L., Lodhi, I. J., Clark, N. A., and Saltiel, A. R. (2012) TC10 is regulated by caveolin in 3T3-L1 adipocytes. *PLoS ONE* **7,** e42451
29. Larkin, M. A., Blackshields, G., Brown, N. P., Chenna, R., McGettigan, P. A., McWilliam, H., Valentin, F., Wallace, I. M., Wilm, A., Lopez, R., Thompson, J. D., Gibson, T. J., and Higgins, D. G. (2007) Clustal W and Clustal X version 2.0. *Bioinformatics* **23,** 2947–2948
30. Kirsch, R. D., and Joly, E. (1998) An improved PCR-mutagenesis strategy for two-site mutagenesis or sequence swapping between related genes. *Nucleic Acids Res.* **26,** 1848–1850
31. Zhang, J.-S., Koenig, A., Young, C., and Billadeau, D. D. (2011) GRB2 couples RhoU to epidermal growth factor receptor signaling and cell migration. *Mol. Biol. Cell.* **22,** 2119–2130
32. Jack, E. R., Madine, J., Lian, L.-Y., and Middleton, D. A. (2008) Membrane interactions of peptides representing the polybasic regions of three Rho GTPases are sensitive to the distribution of arginine and lysine residues. *Mol. Membr. Biol.* **25,** 14–22
33. Laude, A. J., and Prior, I. A. (2008) Palmitoylation and localisation of RAS isoforms are modulated by the hypervariable linker domain. *J. Cell Sci.* **121,** 421–427
34. Källberg, M., Margaryan, G., Wang, S., Ma, J., and Xu, J. (2014) RaptorX server: a resource for template-based protein structure modeling. *Methods Mol. Biol.* **1137,** 17–27
35. Hemsath, L., Dvorsky, R., Fiegen, D., Carlier, M.-F., and Ahmadian, M. R. (2005) An electrostatic steering mechanism of Cdc42 recognition by Wiskott-Aldrich syndrome proteins. *Mol. Cell.* **20,** 313–324
36. Zhang, B., and Zheng, Y. (1998) Negative regulation of Rho family GTPases Cdc42 and Rac2 by homodimer formation. *J. Biol. Chem.* **273,** 25728–25733
37. Lin, W.-C., Iversen, L., Tu, H.-L., Rhodes, C., Christensen, S. M., Iwig, J. S., Hansen, S. D., Huang, W. Y., and Groves, J. T. (2014) H-Ras forms dimers on membrane surfaces via a protein-protein interface. *Proc. Natl. Acad. Sci. U.S.A.* **111,** 2996–3001
38. Rocks, O., Peyker, A., Kahms, M., Verveer, P. J., Koerner, C., Lumbierres, M., Kuhlmann, J., Waldmann, H., Wittinghofer, A., and Bastiaens, P. I. (2005) An acylation cycle regulates localization and activity of palmitoylated Ras isoforms. *Science* **307,** 1746–1752
39. Linder, M. E., and Deschenes, R. J. (2007) Palmitoylation: policing protein stability and traffic. *Nat. Rev. Mol. Cell Biol.* **8,** 74–84
40. Aicart-Ramos, C., Valero, R. A., and Rodriguez-Crespo, I. (2011) Protein palmitoylation and subcellular trafficking. *Biochim. Biophys. Acta* **1808,** 2981–2994
41. Misaki, R., Morimatsu, M., Uemura, T., Waguri, S., Miyoshi, E., Taniguchi, N., Matsuda, M., and Taguchi, T. (2010) Palmitoylated Ras proteins traffic through recycling endosomes to the plasma membrane during exocytosis. *J. Cell Biol.* **191,** 23–29
42. Baker, T. L., Zheng, H., Walker, J., Coloff, J. L., and Buss, J. E. (2003) Distinct rates of palmitate turnover on membrane-bound cellular and oncogenic H-ras. *J. Biol. Chem.* **278,** 19292–19300
43. Goodwin, J. S., Drake, K. R., Rogers, C., Wright, L., Lippincott-Schwartz, J., Philips, M. R., and Kenworthy, A. K. (2005) Depalmitoylated Ras traffics to and from the Golgi complex via a nonvesicular pathway. *J. Cell Biol.* **170,** 261–272
44. Roberts, P. J., Mitin, N., Keller, P. J., Chenette, E. J., Madigan, J. P., Currin, R. O., Cox, A. D., Wilson, O., Kirschmeier, P., and Der, C. J. (2008) Rho Family GTPase modification and dependence on C*AAX* motif-signaled posttranslational modification. *J. Biol. Chem.* **283,** 25150–25163
45. Marcus, K., and Mattos, C. (2015) Direct attack on RAS: intramolecular communication and mutation-specific effects. *Clin. Cancer Res.* **21,** 1810–1818
46. Anderson, E. L., and Hamann, M. J. (2012) Detection of Rho GEF and GAP activity through a sensitive split luciferase assay system. *Biochem. J.* **441,** 869–879
47. Hamann, M. J., Lubking, C. M., Luchini, D. N., and Billadeau, D. D. (2007) Asef2 functions as a Cdc42 exchange factor and is stimulated by the release of an autoinhibitory module from a concealed C-terminal activation element. *Mol. Cell. Biol.* **27,** 1380–1393